Available online at www.sciencedirect.com
SCIENCE DIRECT®
International Journal of Multiphase Flow 30 (2004) 199–216
International Journal of Multiphase Flow
www.elsevier.com/locate/ijmulflow

Preliminary observations of a particle lift force in horizontal slurry flow

Charles S. Campbell *, Francisco Avila-Segura, Zhiwu Liu

Department of Aerospace and Mechanical Engineering, University of Southern California, Los Angeles, CA 90089-1453, USA

Received 23 May 2003; received in revised form 16 October 2003

Abstract

This paper reports experimental observations of an unexpected lift-like interaction force. This force has no apparent analog for single particles in infinite fluids and appears to be a result of multiparticle interactions. The magnitude of this force can be a significant fraction (e.g. 40%) of the total weight of particles in the channel and thus may play a role in flow regime transitions. A simple analysis indicates that the force arises from Bernoulli interaction similar to the mechanism that generates an attraction between particles in a cross-flow.

Keywords: Slurry; Lift; Particle; Force; Interphasial

1. Introduction

Models of multiphase systems usually describe a multiphase flow as interacting continua by writing individual Navier–Stokes like equations for each phase and then couple the equations through interaction terms. For particle–fluid systems, the equations of motion have forms like:

$$(1-v)\frac{\mathrm{D}\mathbf{v}_\mathrm{f}}{\mathrm{D}t} = -(1-v)\nabla P_\mathrm{f} + \nabla\cdot\boldsymbol{\tau}_\mathrm{f} + \boldsymbol{I},$$

$$v\frac{\mathrm{D}\mathbf{v}_\mathrm{p}}{\mathrm{D}t} = -v\nabla P_\mathrm{f} + \nabla\cdot\boldsymbol{\tau}_\mathrm{p} - \boldsymbol{I},$$

* Corresponding author. Tel.: +1-213-740-0498; fax: +1-213-740-8071.
E-mail address: campbell@usc.edu (C.S. Campbell).

0301-9322/$ - see front matter
doi:10.1016/j.ijmultiphaseflow.2003.10.008

where v is the volume fraction (the fraction of a unit volume occupied by particles), $\mathbf{v}_f$ and $\mathbf{v}_p$ are the velocities of the fluid and particle phases, P_f is the fluid pressure (which, as it is the continuous phase, also acts on the particle phase), $\boldsymbol{\tau}_f$ and $\boldsymbol{\tau}_p$ are the stress tensors for the fluid and particle phases respectively exert upon themselves and $\boldsymbol{I}$ is the volume interaction force between the two phases or, in other words, is the force exerted by one phase upon the other. (The exact form of these equations is a matter of debate and often varies from analysis to analysis. These particular forms are presented simply as a point of departure for this discussion and are based on those in Shook and Roco, 1991.)

Typically the interphasial interaction term $\boldsymbol{I}$, is based on forces observed to act on single particles in fluids. Examples are simple drag, added mass, Basset, Saffman, Magnus and other forces. All these forces derive from the relative velocity between the phases known as the "slip velocity" ($\boldsymbol{v}_p - \boldsymbol{v}_f$) and are modeled using extrapolations either from single particle measurements or from experiments performed on fixed or fluidized beds such as the drag force correlations provided by Ergun (1952), Richardson and Zaki (1954) and Foscolo and Gibilaro (1987). It is certainly possible that other forces may be at work in multiparticle systems which arise from interactions between particles, either directly or through the intermediary of the fluid phase. (Such forces can be observed for small numbers of particles in the "drafting, kissing, and tumbling" mechanisms described in, for example, Joseph et al., 1991.) This paper reports observations of a lift-like force that has no apparent analog for single particles and thus must be a result of multiparticle interactions.

2. Experimental setup

This study was performed in a slurry pipe loop which is shown schematically in Fig. 1. The loop is largely constructed of 0.1 m diameter pipe. The 7.3 m test section however, is rectangular in cross-section, with a horizontal dimension of 12.7 cm and a vertical height of 6.35 cm so that the strongest gradients lie in the vertical direction; furthermore, this minimizes errors induced by the secondary flows in the channel corners on the measurement region at the center of the channel. The flow is driven by a Warman 6×4 rubber-lined centrifugal pump, which in turn is driven by a Leeson 30HP AC motor. The motor speed is controlled by a Toshiba variable frequency invertor. A hopper and a series of valves allow particles to be added or removed from the channel in order to control the bulk concentration. A 15 ft stainless steel water-jacketed pipe is used to remove the heat dissipated by the slurry. The flowrate is monitored by a Newsonics electromagnetic flowmeter and the bulk density in the channel is monitored with a small gamma ray densitometer (200 μCi Cs^{137} source collimated into a 0.05 m round beam). The study uses a particle-velocity/fluid-velocity/fluid-pressure/particle-concentration probe that will traverse the test section in the vertical direction as shown in Fig. 2. Details of the probe's construction will be described later. The critical measurements will be made in the last 1.2 m of the test section. All measurements are made along the vertical centerline of the channel to avoid The axial pressure drop will be measured along that section using a Viatran differential pressure transducer with a 3 m H_2O range. The lift force will be ascertained from measurements of the fluid pressure difference made either between the top and bottom of the square test section or between the top of the channel and a small pressure port mounted in the movable probe as shown in Fig. 2. That pressure difference is

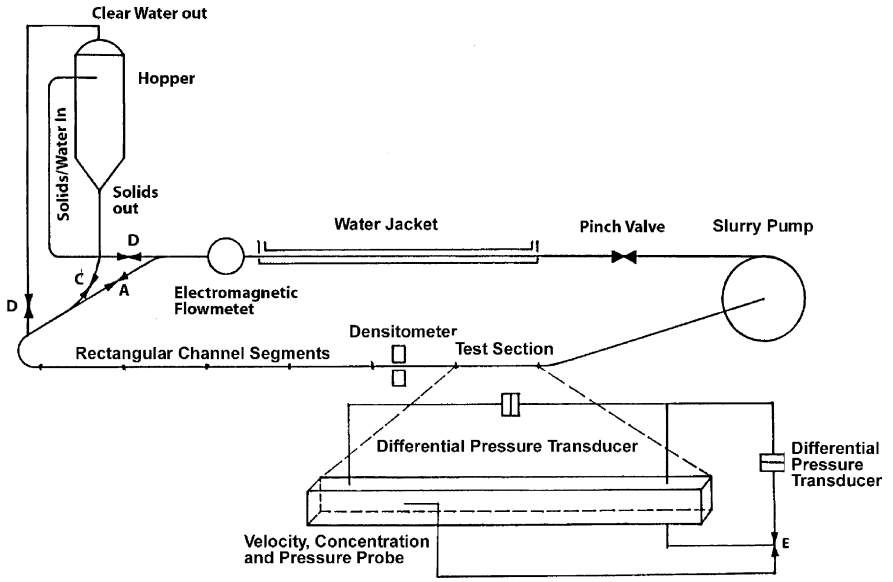

Fig. 1. Schematic of the slurry apparatus.

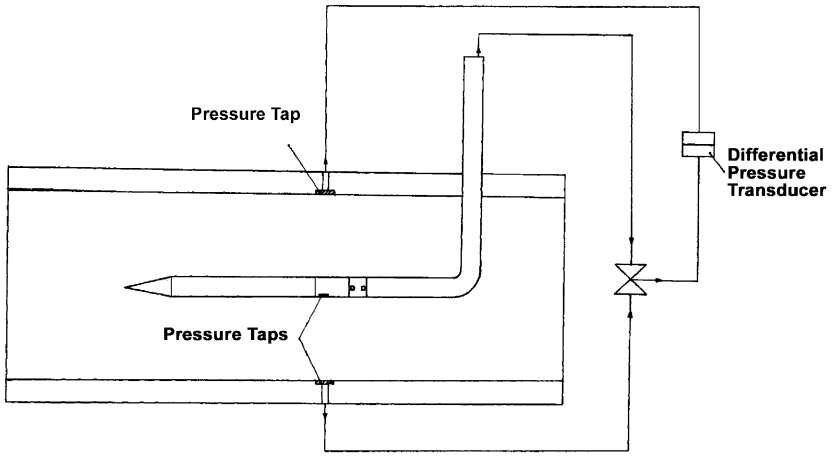

Fig. 2. A schematic of the pressure hookup between the pressure tap on the probe and hose on the top and bottom walls of the test section.

determined by a Viatran differential pressure transducer calibrated within a range of 0–0.127 m of water column. To keep them free of particles, the pressure taps to the channel are made through porous plates. Data are sampled using an RC electronics data acquisition card mounted in an IBM PC compatible computer. The bulk conductivity of the liquid within the loop is continually monitored by a YSI model 35 conductance meter connected to a flow-through conductance cell through which a small part of the liquid flow is diverted. The concentration probe is calibrated

against the conductivity of the liquid and this allows accurate measurement in cases where due to changes in temperature and other factors might affect the measurements.

3. The unexpected lift force

This loop was built for an investigation into the mechanisms by which heavy settling particles in a slurry are maintained in a fluidized state. Two such mechanisms have been identified: (1) entrainment of particles in the turbulent eddies of the fluid (particle–fluid interactions) and (2) self-fluidization through particle–particle interactions such as is active in dry granular flows (e.g. the dispersive stresses, first identified by Bagnold, 1954).

The original idea behind these fluidization mechanism experiments was very simple. The determination is simply made with a differential pressure measurement between the top and bottom of a rectangular channel using the hookup shown in Fig. 2. If particles are entrained in the turbulence of a fluid, a simple force balance indicates that the weight of the suspended particles will appear as an increase in the apparent weight of the fluid which will be reflected in the pressure measurement. (At least that would be the case if there were no lift-like forces that acted between the phases.) Thus, if one knows the pressure difference and the average concentration of solid material in the channel, one should be able to infer the fraction of particles that are suspended within the fluid turbulence and conclude that the rest must be supported by particle–particle interactions.

The results of this study were both very encouraging and somewhat surprising. Overall, they indicate that the dominant fluidization mechanism determines whether the flow demonstrates homogeneous or heterogeneous behavior and along the way, explain a curious engineering observation. The engineering criterion for distinguishing between the heterogeneous and homogeneous flow regimes (see, for example, Derammelaere and Wasp, 1984) is largely determined by particle size and weight (i.e. the susceptibility of a particle to fluid forces) and is relatively independent of flow velocity. Early experimental results (see Campbell and Avila-Segura, 1990) showed that homogeneous flows are associated with entrainment of particles in the fluid turbulence and thus are associated with small and light particles that are highly susceptible to fluid forces. Heterogeneous flows are associated with support by particle interactions and thus with larger and heavier particles relatively immune to fluid forces.

However, the results associated with heterogeneous flows were very surprising. Fig. 3 shows an example of the raw measurement of the fluid pressure difference, Δp_f, between the top and bottom of the channel, taken from tests on 0.5 mm glassbeads which, generally, exhibit heterogeneous behavior (i.e. the majority of the particles rides as a dense mass along the channel bottom, leaving a nearly particle-free region towards the top of the channel). Here, $\Delta p_f = (p_H - p_0) - 2\rho_f g H$, where p_H is the pressure measured through a tap at the top of the channel (see Fig. 2), p_0 is the pressure measured through the tap at the bottom of the channel, ρ_f is the liquid density (for water used here 1000 kg/m^3), g is the gravitational acceleration and H is the height of the channel (here 6.35 cm). This plot shows that the global fluidization behavior is really quite complicated. As the liquid flow rate is increased from zero, the measured pressure difference begins to rise as particles are entrained in the liquid. In this region, the particles are moving in a saltated layer over a largely stationary bed of particles and the measured pressure difference is an indication of the increasingly

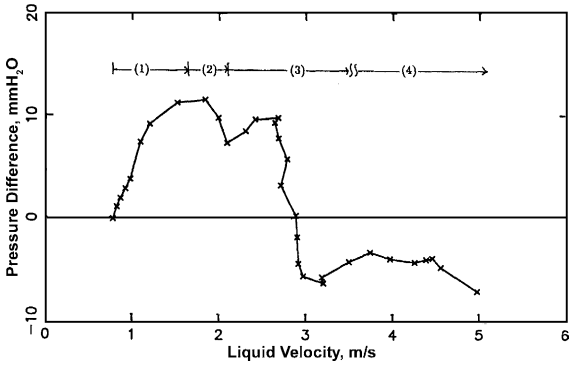

Fig. 3. The pressure difference between the top and bottom of the channel for 0.5 mm glassbeads at a 35% mean solids concentration. The numbers refer to various flow regimes. (1) Saltated flow, (2) pulsatile dune motion, (3) complete dune motion, (4) fully heterogeneous flow. Note that the pressure goes negative in the fully heterogeneous region indicating a lift force pressing the particles against the bottom of the channel.

larger number of particles supported by the fluid. Eventually, the whole particle mass begins to move and the pressure difference drops off indicating the overwhelming importance of particle–particle interactions as a fluidization mechanism. In between, the behavior becomes quite complicated due to changes in the flow regime.

The shape of the curve in Fig. 3 may be directly related to the character of the flow. For the purposes of illustration, the curve has been divided into four segments. For the low velocities, labeled (1), the solid material moves in a saltated layer over a largely stagnant bed. Now, in this region, the surface of the stagnant bed forms into a wavy pattern by a natural instability that is reminiscent of the way that sand dunes are formed. The water flow must accelerate in order to pass over the top of the dune and easily entrains solid material. But the flow separates on the other side of the hump, forming a large vortex which redeposits the material on the other side, causing a slow motion of the dune body. During this process, the large majority of the constituent particles remain stationary. The spacing between the dunes is very regular and appears to be largely determined by the size of the separated vortex. But the flow separation also causes a large pressure drop across the dune itself which, with increased liquid flowrate, eventually becomes large enough to cause the dune to move as a whole. The onset of dune motion corresponds to the first maximum in the Δp_f curve. However, because of the nature of its source, the motion is not continuous, but moves in a stop and go fashion with the particles coming to a complete halt in the valleys between the dunes. This region is labeled (2). This state of motion occurs because the majority of the pressure drop occurs across the dunes while a much smaller pressure drop occurs in the wider expanse of the valleys. Consequently, the dunes are in continuous motion, but, as the dunes move with a noticeable velocity gradient through their height, they leave basal material behind. When the basal material enters a valley, it experiences a smaller pressure drop and comes to a halt, resulting in the observed stop and go motion. This state of motion coincides with a drop in Δp_f, which, once again, may be explained by the reduced relative velocity between the fluid and particles. The condition corresponding to region (3) is a direct extension of that in region (2). Here, however, the entire body of material is continuously moving, although the surface of the particle bed retains its dune-like shape and all of the mechanisms referred to above are still active;

as a result, the solid material moves with a noticeably pulsatile fashion, slowing down when in a valley and speeding up when in a dune, but never coming to a halt. Here the pressure difference, Δp_f, again rises with increasing fluid velocity, although, eventually, particle dispersive forces begin to take hold and Δp_f begins to drop off. Somewhere in the subsequent evolution of the flow, the dune-like structure disappears and the flow develops a nearly uniform heterogeneous character. However, at this stage, the flow in moving so rapidly that it is difficult to visually determine exactly when the dunes have disappeared and the heterogeneous character has developed. (In Fig. 3, the line between the points is drawn in order of increasing pump power. As some of the power goes to drive the particle phase motion, increasing the power does not necessarily mean an increase in the liquid velocity. Thus there are some cases in Fig. 3, particularly near flow regime changes where the state of particle motion is changing, in which successive points show slightly smaller liquid velocities than their predecessors.)

The most surprising part of this data is that, at the larger liquid flow velocities, the Δp_f actually go negative. In the context of the discussion presented above, a negative Δp_f indicates that the particles support the fluid, rather than the other way around. This would require some previously unknown interaction force between the particles and the fluid. At first, this made us doubt our measuring technique. As the Δp_f measured in these experiments is a fraction of a percent of the stagnation pressure of water, any small misalignment of the porous plates used to cover the pressure taps may induce inertial pressure differences. Numerous attempts were made to correct this problem by realigning the porous plates. Eventually though, we purposely oriented the plates so that, with water only, we observed a positive pressure difference when no particles were present, yet, when particles were added, the pressure drop still went negative at the larger liquid flow velocities. From this, we conclude that the negative Δp_f are not caused by measurement errors, but instead, represent some unexplained interaction between the particles and the fluid.

A preliminary attempt was made to locate the source of these negative pressures. In order to sample the local fluid pressure, a small pressure tap is inserted in the bottom of a probe that contained two electrode pairs for an impedance velocity/concentration measurement (see Fig. 2). The particle concentration is determined by a time averaged value of the signals produced by any of the electrodes (similar to Nasr-El-Din et al., 1987) and the particle velocity is found by cross-correlating those signals using a standard time-of-flight technique (similar to Savage, 1979; Ishida and Shirai, 1979; Brown and Shook, 1983; Ahn et al., 1991). For these measurements, the electrodes were excited by a special set of fluid impedance measuring electronics which were modified versions of those used by Ceccio (1990) which were in turn, derived from those used by Bernier (1981). The probe electronics are connected to a data acquisition board installed in an IBM compatible computer. The pressure tap on the probe is connected to a differential pressure transducer (as shown in Fig. 2) which allows the system to measure either the pressure between the probe and the top of the channel or between the pressure taps at the top and bottom of the channel. One example, (for 1 mm glassbeads at a concentration of $\bar{\nu} = 0.25$, averaged over the cross-section of the channel, and at a mean water flow velocity of 4.1 m/s) is illustrated in Fig. 4. This particular case was chosen both because it illustrates many of the features we have seen in these flows. The three panels show the variation of velocity, particle concentration and pressure difference Δp_f (plotted relative to an equivalent length of water column). At each position y, $\Delta p_f = (p_H - p_y) - 2\rho_f g(H - y)$, where p_H is the pressure measured through a tap on the top of the channel at height H (here equal to 6.35 cm), p_y is the pressure measured from the tap on the probe

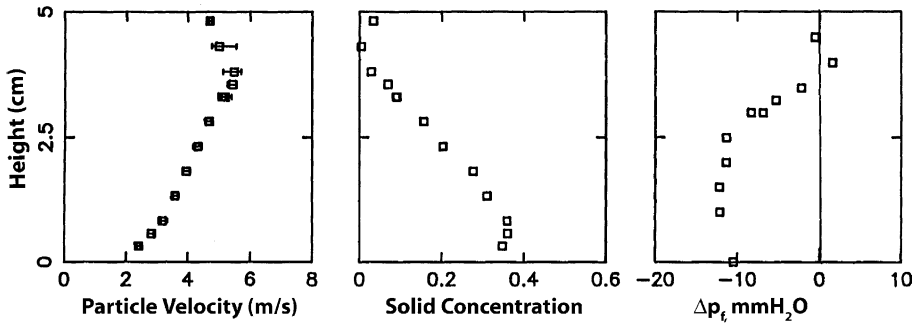

Fig. 4. An example of the measurement of velocity, concentration and pressure difference across the channel. This case is for a mean particle concentration $\bar{v} = 0.25$ at a mean liquid flow velocity of about 4.1 m/s. Note the top of the channel is located off-scale at 6.35 cm.

at position y, ρ_f is the liquid density (here for water, $\rho_f = 1000$ kg/m^3) and g is the gravitational acceleration.

Note that the pressure profile shows a small region of positive pressure near the top of the channel, indicating that in that region, particles are entrained in the fluid turbulence. But for the most part, the pressures are negative. However, through the densest regions of the bed, the pressure does not change. The source of the negative pressures appears to be in the region of small concentrations (between about 5% and 20%) lying between the nearly particle-free liquid flow at the top of the channel and the dense particle flow below. At the large concentrations near the channel bottom, there will be a large resistance to relative motion of the fluid, and one would expect small slip velocities. At small concentrations near the channel top, where particle–particle interactions are infrequent, nothing holds the particles back, and so they will move with nearly the same velocity as the liquid. But at moderate concentrations where the lift force is active, there will be sufficient interparticle interactions to retard the particles, yet the interparticle spacing will be wide enough to not significantly retard the liquid, and a significant slip-velocity between the phases can be expected. This indicates that the interaction may well be a lift-like force driven by the slip velocity.

Three more examples are shown in Fig. 5. These three cases, once again for 1 mm glassbeads, were taken for three different mean particle concentrations, $\bar{v} = 0.17$, 0.27 and 0.40, all three taken at similar liquid flow velocities, (although those velocities are slightly larger than that shown in Fig. 4). All of these show nearly the same phenomena: i.e. any positive pressure differences are generated by the small fraction of particles entrained in the nearly particle-free zone near the top of the channel where the fluid velocity is largest, while the negative pressures are generated in the moderate concentration zone between the particle free and dense regions where the slip-velocity between the particle and the fluid should be greatest. Finally in the dense heterogeneous layers, the fluid pressure is nearly constant, indicating that all of the material is supported by particle–particle interactions.

While these negative pressures might appear to be a small effect, they turn out to be quite significant when compared to the weight of the particles. For example, the case shown in Fig. 4 demonstrates a pressure drop of −10 mm of water across the channel. The weight of particles per unit area (taking into account buoyancy effects) is $\bar{v}(\rho_p - \rho_f)gH$, where $\bar{v}$ is the average particle

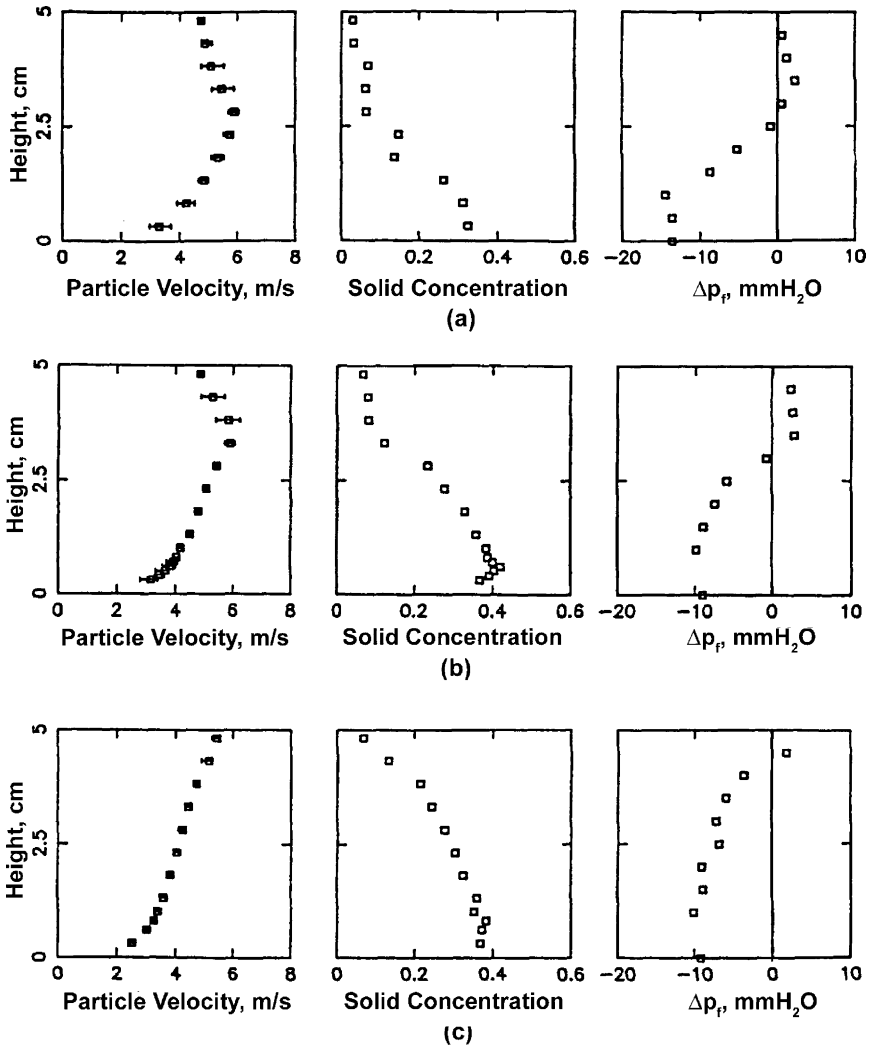

Fig. 5. Three examples of the velocity/concentration/pressure measurement. All cases were taken for 1 mm glassbeads. (a) $\bar{v} = 0.17$, mean liquid flow velocity = 4.7 m/s; (b) $\bar{v} = 0.27$, mean liquid flow velocity = 4.4 m/s; (c) $\bar{v} = 0.4$, mean liquid flow velocity = 4.2 m/s.

concentration and ρ_p is the particle density (here, 2500 kg/m^3). Using the values representative of Fig. 4, the total particle weight per unit wall area is only about 24 mm of water, making the negative pressures about 40% of the total particle weight. This is particularly significant because the entire pressure change occurs across a narrow section of the bed that contains only about one-eighth of the total particles present. In that case the vertical pressure difference across that section is about 3 times the weight of particles contained there. Consequently, this interaction force can significantly affect the behavior near the interface between the region of nearly clear fluid and the relatively dense heterogeneous layer. Thus it does not seem unreasonable to suspect that this lift-like force might be responsible for flow regime transitions such as the transition during which

dune-like structures disappear and the flow adopts a fully heterogeneous behavior. As the force works to press particles against the walls, it may also be responsible for annular flow transitions in vertical flows and may stabilize such flows once formed.

4. Slip velocity probe design

To better understand this strange force, we have built a test probe to measure the slip-velocity. The basic idea for the probe design is shown in Fig. 6. Two electrode pairs are used to sense the local impedance of the fluid. These will serve double duty. First, the average value of the local impedance will be used to determine the particle concentration. Then the cross-correlation of the two signals will provide the particle velocities. Then, a pulsed injection of a high conductivity fluid (e.g. concentrated salt water) through the injection port will induce impedance changes in the fluid itself that can be sensed at the electrodes and used to determine the fluid velocity. The tracer injection scheme is shown in Fig. 6 and uses a solenoid valve triggered by a computer to feed the salt solution to the probe. The storage tank is pressurized by lab air which will control the feed rate of the salt water mixture. The strength of the injection and the spacing between the injection point have been carefully chosen through many tests in a drag tank to not disturb the surrounding fluid and to allow the tracer to accelerate to the surrounding flow speed before the velocity is sensed.

At first glance one might think that there is a natural error in the liquid-velocity measurement technique arising from the boundary layer that invariably forms around the probe. This implies that the liquid velocity in the immediate neighborhood of the electrodes (the region in which they will be most sensitive) will be smaller than that far away thus introducing an error into the velocity measurement. (Less error would be expected in the particle measurement as the particles slip along the probe surface while, at least microscopically, the fluid must show no-slip there.) However, this is not true because of the interaction between diffusion and the flow of the saltwater tracer. This process was first studied by Taylor (1953, 1954a,b) for both laminar and turbulent flow. He was intrigued by a tried and true method for measuring water flowrates (used by the London water district among others) by injecting salt water into the lines and then, via a conductivity measurement, detect its passage at some point downstream (much the same technique

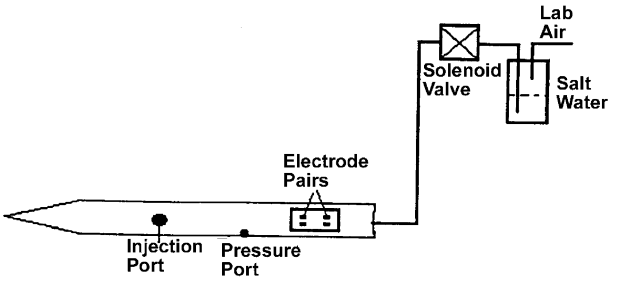

Fig. 6. A schematic of the probe used to measure the particle concentration, particle velocity, liquid velocity and vertical pressure gradient.

used here). One's first guess would be that the signal would move at the maximum velocity in the pipe, but in practice, it was experimentally found (Allen and Taylor, 1923) to give a very accurate measurement of the average velocity. Taylor's (1953, 1954a,b) analyses supported that somewhat surprising conclusion. This can be understood physically by considering the following scenario. Suppose one injects a plug of saltwater, or other "tagged" fluid, that fills a cross-section of a pipe. The velocity profile in the pipe will tend to stretch the plug with the high velocity fluid at the center leaving behind the low velocity fluid at the walls. But that results in a strong radial concentration gradient that diffusion will try and eliminate. Following the high velocity fluid at the center, one would soon find a high concentration region near the center surrounded by nearly zero concentration at the walls. The resulting large concentration gradient causes tagged fluid to rapidly diffuse outwards towards the lower velocity region at the wall, so that the tagged fluid fills the pipe. Conversely, if one follows the plug of tagged fluid near the wall, which has nearly zero velocity, it will soon surround a central core of nearly zero concentration; that induces a huge concentration gradient which will cause tagged material to diffuse rapidly inwards towards the high velocity region near the pipe center again filling the pipe with tagged fluid. Consequently, whenever the velocity gradient tries to disperse the plug of tagged fluid, diffusion works to move the tagged material towards regions that move with the average velocity in the pipe. (Chatwin and Allen, 1985, has a nice discussion of this process.) The result is a plug of tagged material whose centroid moves with the average velocity (although the velocity profile does stretch out the length of the tagged section). Batchelor (1964) analyzed the corresponding situation for a boundary layer and showed that the plug of tagged material moved with the velocity appropriate to the position of the plug's center of mass. While Batchelor left many undetermined constants in his theoretical analysis, the general predictions of the theory have been confirmed experimentally (e.g. Shillen and Corrsin, 1975). Consequently, the key to making an accurate fluid velocity measurement using this technique is to inject the fluid so that it's center of mass lies in the undisturbed fluid outside the boundary layer that forms on the probe. As the boundary layer is thin, this should be easy to accomplish. Thus, the signal sensed by the electrodes will accurately measure the velocity of the undisturbed fluid.

5. Preliminary measurement

Unfortunately, we were only able to obtain one set of data before the apparatus had to be dismantled and placed in storage. The results are shown in Fig. 7 for a 20% concentration of 0.5 mm glassbeads with a mean liquid velocity of 4.1 m/s. The figure shows separate plots for the liquid and particle velocities, the pressure profile, the concentration and the slip velocity. Note that only the bottom 2/3 of the channel are shown here. In looking at the velocity figures, it is important to note that the center of the channel lies about 3.18 cm from the bottom which roughly corresponds to the maximum in the velocity profiles and that the height of the channel is 6.35 cm, slightly above the top of each plot. Another interesting thing to note is that there is significant slip at the lower wall for both the particle and liquid velocities. It is not surprising that the particles slip at the wall, and given that, it appears that the fluid shows nearly no-slip with the particle phase, not no-slip with the wall. Finally notice that the maximum slip velocity occurs at a concentration of about 17% by volume, which is in the range where the negative pressures were

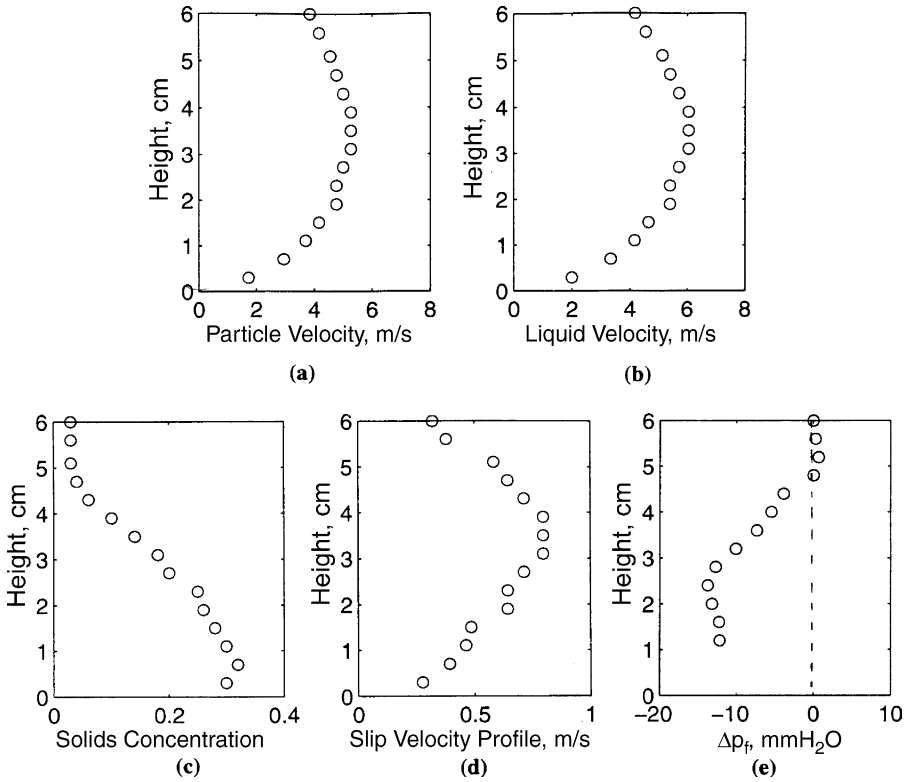

Fig. 7. Measurements of (a) liquid velocity, (b) particle velocity, (c) particle concentration, (d) slip velocity and (e) pressure gradient for a 20% average concentration of 0.5 mm glassbeads in water moving at a mean velocity of 4 m/s. In these graphs, the middle of the channel is 3.18 cm from the bottom and the top of the channel is at 6.35 cm.

observed in Figs. 4 and 5. Note also that the slip-velocity goes to zero in the higher concentration regions and in the regions of nearly zero concentration. The measured slip velocities are quite large, with a maximum of about 0.8 m/s.

6. A physical explanation for the lift force

So far, it appears that the negative pressures are probably a result of some kind of lift-like (in this case, negative lift) particle–fluid interaction. However, it is unlikely that it could be accounted for by the single-particle interaction forces that were mentioned in the introduction. The two lift forces mentioned there are the Saffman force and the Magnus force. As the Saffman force is restricted to low particle Reynolds numbers, it will not be present in 0.5 mm particle systems and 0.8 m/s slip velocities. That leaves only the Magnus force. But again, that is an unlikely explanation due to the direction of the force. The particle velocity profiles indicate that the velocity gradient is positive in the regions where the pressure goes negative. A positive velocity gradient will induce a clockwise rotation of the particles and the consequent clockwise circulation in the fluid will generate a positive and not a negative lift on the particle.

The only Magnus-like mechanism that points in the right direction is seen for smooth surfaced rotating particles when the surface rotational velocity is small compared with the fluid-particle slip velocity. This results from a reorientation of the separation zone behind the particle (Clift et al., 1978). In order for a Magnus-like mechanism to be active, the surface velocity $R\omega$ (where R is the particle radius and ω is the angular rotation rate) must be smaller than about 40% of the slip velocity. The rotation rate ω, is approximately 1/2 the particle shear rate times the diameter and thus can be approximated from the particle velocity profile. But examining the pressure profile in Fig. 7e shows that the region where the lift force is active (which is associated with the positive vertical pressure gradient near the center of the channel, 3–4 cm from the bottom) corresponds to the region of largest slip velocity which is also a region where the particle velocity gradient is near zero. Hence one expects no particle rotation in that region and thus these observations cannot be explained by a Magnus force.

Lubrication forces cannot play a part the relatively small concentrations (5–30%) at which the lift force is active. A 30% concentration of spheres corresponds to a mean spacing between the particle surfaces of about $0.4R$ or about 100 μm, two to three orders of magnitude larger than the submicron separations at which lubrication forces become active. Note also that the mean particle separation is larger than the boundary layer thickness which can be estimated for these particles and slip velocities from the Blasius series solutions in Schlichting (1979) at 35 μm. As a result a good part of the flow between the particles will be largely inviscid.

It is our belief that the observed force has no analog for a single particle in a fluid and is the result of multiparticle interactions. One such mechanism that suggests itself is derived from the Bernoulli effect that draws together particles which are oriented perpendicular to a cross-flow. Consider an infinite line of particles as shown in Fig. 8. In all the cases where the lift force has been observed, there is a negative vertical concentration gradient. Thus the concentration decreases and the gaps between particles become larger moving upwards along the column. As a result, the velocity through the larger gap above the particle will be smaller than through the tighter gap below. Bernoulli dictates that the pressure above the particle will be larger than that below. Continuing this idea downward along the chain, would generate a monotonically decreasing pressure—in other words, a positive vertical pressure gradient just as was observed above. One can expect there to be limits on the concentrations for which this effect can be observed. At very low concentrations, the particles will be widely spaced and will have little effect on the liquid flow about one another. At very high concentrations one can guess that the slip velocity will become small and eliminate the pressure gradient.

This process has been studied for two-particles (e.g. Kim et al., 1993). The results show that the force is attractive at larger separations (Fig. 9a), but becomes repulsive when the particles become very near (Fig. 9b). However, the argument in the last paragraph depends on the force always being attractive between the particles in the column in Fig. 8. For two particles, the fluid has a choice of whether to pass through the narrow gap between the particles or to pass around them to the outside (Fig. 9). If the gap becomes very narrow as in Fig. 9b, it will restrict the flow and more fluid will choose to pass around to the outside of the particle. This will reduce the velocity in the gap and will rotate the stagnation point (the point of largest pressure) towards the gap as illustrated in Fig. 9b. The reduced velocity in the gap along with the rotation of the stagnation point will result in a repulsive force that will push the particles apart. In the particle column with a concentration gradient (Fig. 8), no such path of least resistance will exist and all of the fluid will be

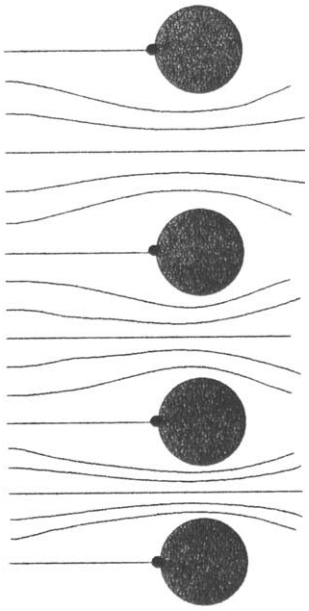

Fig. 8. The fluid acceleration in a long line of particles within a concentration gradient. Here, the particles are more widely spaced as one moves upwards (i.e. there is a negative vertical concentration gradient, just as in the slurry experiments). When the mean concentration is small enough, the fluid will move faster and produce a lower pressure in the thinner gaps, producing a positive pressure gradient.

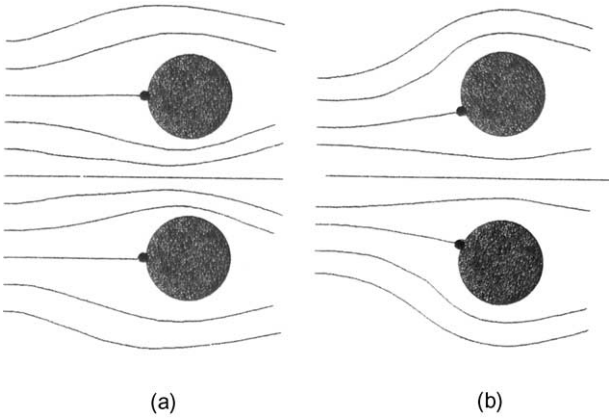

Fig. 9. A schematic diagram of the Bernoulli effect between two particles in a cross-flow. (a) When the particles are "widely" spaced, the flow moves faster with a corresponding pressure deficit between the particles. This results in the particles being drawn together. (b) When the particles draw close together, it is difficult for fluid to move between them. As a result, the stagnation points move toward the center which pushes the particles apart.

forced to pass through the interparticle gaps. In these cases there will be no rotation of the stagnation points and, hence, no repulsive forces and only the attractive forces exist. Thus, these Bernoulli interactions have the potential to explain the unexpected lift force.

7. A simple analysis

A simple calculation will demonstrate that the Bernoulli force theory is the most likely explanation for the lift force. To do this exactly would require finding the flow field through a mass of moving particles, a hopelessly complicated task. But the goal here is not to exactly model the flow, just to give support to the speculation in the last paragraph. Thus, simply assume that as the flow moves between particles, it must accelerate as required to pass through the gap. If the spacing between particles centers is s ($s = (\frac{4}{3}\pi/v)^{1/3}R$, where R is the particle radius), then between two corresponding points at an angle ζ on the sphere surface (see Fig. 10), the separation is $(s - 2R\cos\zeta)$. The fluid that originally moved in the spacing s must now squeeze through the gap, so to first approximation continuity requires $u_s s = u_1(s - 2R\cos\zeta)$, where u_s is the slip velocity far away and u_1 is the velocity in the gap. So:

$$u_1 = u_s \frac{s}{(s - 2R\cos\zeta)}. \tag{7.1}$$

According to Bernoulli:

$$p + \frac{1}{2}\rho u_1^2 = p_0 + \frac{1}{2}\rho u_s^2, \tag{7.2}$$

where p is the local pressure and p_0 is the pressure far away. The average pressure on the lower surface of the sphere is then

$$\begin{aligned}\bar{p} &= p_0 + \frac{1}{2}\rho(u_s^2 - \bar{u}_1^2) \\ &= p_0 + \frac{1}{2}\rho u_s^2 - \frac{1}{2}\rho\left(\frac{1}{2\pi R^2}\int_0^{\pi/2} u_s^2\left(\frac{s}{(s - 2R\cos\zeta)}\right)^2 2\pi R^2 \sin\zeta\,\mathrm{d}\zeta\right),\end{aligned} \tag{7.3}$$

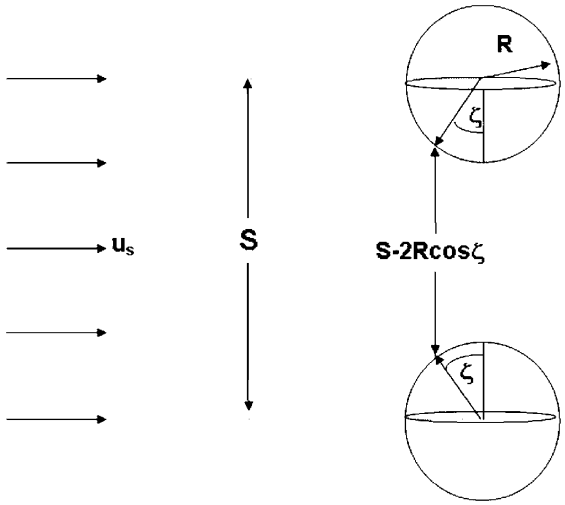

Fig. 10. The geometry used to predict the fluid acceleration between two spheres in a cross-flow.

$$\bar{p} = p_0 + \frac{1}{2}\rho u_s^2\left(1 - \frac{s}{(s-2R)}\right) = p_0 - \frac{1}{2}\rho u_s^2\left(\frac{2R}{(s-2R)}\right). \tag{7.4}$$

Since both the slip velocity u_s and concentration v (and thus the spacing s) vary with the vertical position, y (see Fig. 11), we expand about the center of one particle retaining only first order terms:

$$\bar{p} = p_0 - \frac{1}{2}\rho u_{s\perp}^2\left(\frac{2R}{(s_0-2R)}\right) - \rho u_{s\perp}\left(\frac{2R}{(s_0-2R)}\right) y\frac{\mathrm{d}u_s}{\mathrm{d}y} + \frac{1}{2}\rho u_{s0\perp}^2\left(\frac{2R}{(s_0-2R)^2}\right) y\frac{\mathrm{d}s}{\mathrm{d}y}. \tag{7.5}$$

Here we introduce the notation $u_{s\perp} = u_{s0}\sin\theta$ to denote the slip velocity perpendicular to the line connecting the particle centers defined at the location of the particle at the origin in Fig. 11 (as only the perpendicular component is accelerated while moving through the particle gap). The symbol s_0 is the mean particle spacing corresponding to the concentration defined at the center of the particle at the origin and u_{s0} the slip velocity at the same location. Hence in linearizing (7.4) to yield (7.5), it is assumed that $u_s = u_{s0} + y\frac{\mathrm{d}u_s}{\mathrm{d}y}$ and $s = s_0 + y\frac{\mathrm{d}s}{\mathrm{d}y}$, where $y = \frac{s_0}{2}\sin\theta\cos\phi$ is the vertical coordinate of the point midway between the centers of the spheres.

Now the two spheres need not be oriented vertically with the line between their centers perpendicular to the flow. To first approximation they can be assumed to have random orientation as shown in Fig. 11.

The next goal is to compute the net pressure force acting on the sphere in the y-direction. To do this we need to compute $\int -\bar{p}n_y\,\mathrm{d}A$ over the surface of the sphere. Here $n_y = \sin\theta\cos\phi$. Note that the first two terms in (7.5) are constants and will integrate to zero. Thus the net pressure force on the sphere acting in the y-direction is

$$\begin{aligned} F_y = &\int_0^{\pi}\int_0^{2\pi} -\rho(u_{s0}\sin\theta)\left(\frac{2R}{(s_0-2R)}\right)\left(\frac{s_0}{2}\sin\theta\cos\phi\right)\frac{\mathrm{d}u_s}{\mathrm{d}y}(\sin\theta\cos\phi)R^2\sin\theta\,\mathrm{d}\theta\,\mathrm{d}\phi \\ &+ \int_0^{\pi}\int_0^{2\pi}\frac{1}{2}\rho(u_{s0}\sin\theta)^2\left(\frac{2R}{(s_0-2R)^2}\right)\left(\frac{s_0}{2}\sin\theta\cos\phi\right)\frac{\mathrm{d}s}{\mathrm{d}y}(\sin\theta\cos\phi)R^2\sin\theta\,\mathrm{d}\theta\,\mathrm{d}\phi. \end{aligned} \tag{7.6}$$

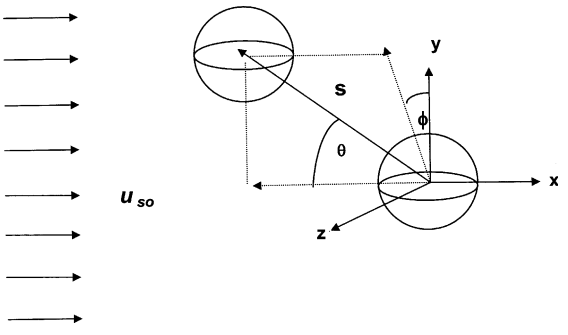

Fig. 11. The orientation of two spheres in spherical coordinates. All orientations are assumed to be equally probable.

So:

$$F_y = -\left(\frac{3\pi^2}{8}\rho u_{s0} s_0 \frac{R^3}{(s_0 - 2R)}\right)\frac{\mathrm{d}u_s}{\mathrm{d}y} + \left(\frac{8\pi}{15}\rho u_{s0}^2 s_0 \frac{R^3}{(s_0 - 2R)^2}\right)\frac{\mathrm{d}s}{\mathrm{d}y}, \tag{7.7}$$

the above is the force on a single particle. Given that there are $n = (v/\frac{4}{3}\pi R^3)$ particles per unit volume, and that the force on the fluid is the negative reaction to the force on the particle, this generates a pressure gradient:

$$\frac{\mathrm{d}p}{\mathrm{d}y} = -nF_y = \left(\frac{9\pi}{32}\frac{\rho v u_{s0} s_0}{(s_0 - 2R)}\right)\frac{\mathrm{d}u_s}{\mathrm{d}y} - \left(\frac{2}{5}\frac{\rho v u_{s0}^2 s_0}{(s_0 - 2R)^2}\right)\frac{\mathrm{d}s}{\mathrm{d}y}. \tag{7.8}$$

This may be integrated using the experimental data for u_{s0} and v (using the relationship $s_0 = (\frac{4}{3}\pi/v)^{1/3}R$) in Fig. 7 to obtain the pressure profile. The integration is performed with a simple trapezoidal rule with the derivatives approximated by simple differencing between the experimental points. To correspond to Fig. 7, $\rho = 1000$ kg/m^3 and $R = 0.00025$ m. The result is shown in Fig. 12.

Note that the integration will require a single boundary condition on the pressure. The most obvious choice would be to specify the pressure as zero near the top of the channel. But this model does not include the lift due to turbulent entrainment and hence the physics are incomplete for that region of the channel. Thus, for comparison purposes the theory is referenced at the fourth point from the top which lies at the start of the zone of negative pressure. This line not only qualitatively follows the pattern of the pressure, but except for the bottom point gives reasonable quantitative predictions of the pressure profile.

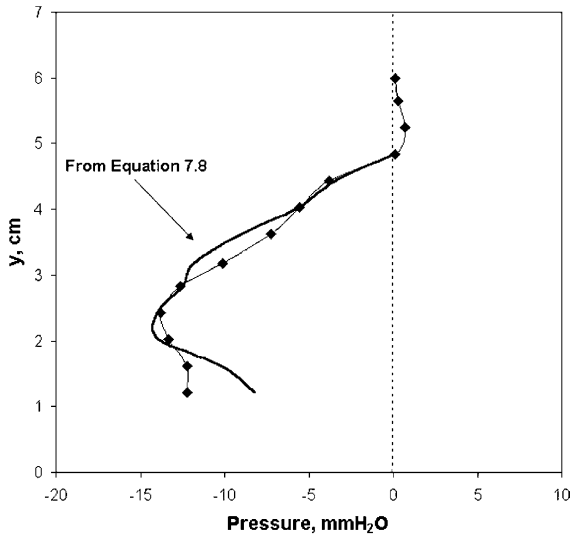

Fig. 12. A comparison between the pressure profile data from Fig. 7e and that predicted by integrating Eq. (7.8) using the experimental concentration and slip velocity profile from Fig. 7c and d.

The comparison between theory and experiment is surprisingly good considering the crude nature of the model. That comparison gives strong evidence that the force results from exactly the kind of Bernoulli interaction described in the last section.

8. Conclusions

This paper has presented preliminary observations of a lift force in heterogeneous horizontal slurry flows. The force was detected by measuring the vertical pressure distribution across the channel. A positive pressure relative to the hydrostatic head of water-only, would indicate that particles are supported by fluid turbulence. Indeed such positive pressures were observed in the dilute regions near the top of the channel. However, in denser regions nearer to the bottom of the channel, the pressure went negative indicating that the particles were supporting the fluid, not the other way around! This indicated the action of a negative lift force pressing the particles towards the bottom of the channel. The force was surprisingly large, about 40% of the entire weight of particles in the channel, and about three times the weight of particles in the narrow region where the force is active. By pressing down on the tops of dune-like structures, the force may be responsible for their disappearance and thus partially account for the transition from moving-dune to fully heterogeneous flows. Also, although annular flows were not studied here, the force presses particle towards the walls; thus in an annular flow situation, the force would help support particles against the top of a pipe and thus may be partially responsible for the annular flow transition.

The force is associated with regions of large slip velocity, moderate particle concentrations and negative vertical concentration gradients. On that basis, it was hypothesized that this was a Bernoulli effect. Due to the negative concentration gradient, the fluid is forced to move faster through the narrow gaps below a particle than through the wider gap above; following Bernoulli, the pressure is smaller below the particle forcing the particle downwards, thus resulting in a positive fluid pressure gradient. A simple analysis based on these ideas was surprisingly successful in predicting the experimental pressure profile. Note that this force depends on the presence of many particles in the flow and, unlike the forces used in most multiphase modeling, has no analog for a single particle in an infinite fluid.

Acknowledgements

The authors would like to acknowledge the support of the US Department of Energy under grant DE-FG22-86PC90957 and the National Science Foundation under grant CTS-8907776.

References

Ahn, H., Brennen, C.E., Sabersky, R.H., 1991. Measurement of the velocity, velocity fluctuation, density and stresses for chute flows of granular material. J. Appl. Mech. ASME 58, 792–803.

Allen, C.M., Taylor, E.A., 1923. The salt velocity method of water measurement. Trans. Amer. Soc. Mech. Eng. 45, 285–341.

Bagnold, R.A, 1954. Experiments on a gravity-free dispersion of large solid particles in a Newtonian fluid. Proc. Roy. Soc. Lond., Ser. A 225, 49–63.

Batchelor, G.K., 1964. Diffusion from sources in a turbulent boundary layer. Arch. Mech. Stos. 16, 661–670.

Bernier, R.J.N., 1981. Unsteady two-phase flow instrumentation and measurement. PhD Thesis and Report No. E 200.4, California Institute of Technology, Pasadena, CA, USA, 152pp.

Brown, N.P., Shook, C.A., 1983. A probe for point velocities in slurry flows. Can. J. Chem. Eng. 61, 507–602.

Campbell, C.S., Avila-Segura, F.A., 1990. Particulate fluidization in horizontal slurry flow. In: Proceedings NSF-DOE Workshop on Flow of Particulates and Fluids, Gaithersburg, MD, October 1–3, 1990, pp. 167–176.

Ceccio, S.L, 1990. Observations of the dynamics and acoustics of traveling bubble cavitation. PhD thesis and Report No. Eng 249.11, California Institute of Technology, Pasadena, CA, USA, 158pp.

Chatwin, P.C., Allen, C.M., 1985. Mathematical models of dispersion in rivers and estuaries. Ann. Rev. Fluid Mech. 17, 119–149.

Clift, R., J.R, Weber, M.E., 1978. Bubbles, Drops, and Particles. Academic Press, New York. 380pp.

Derammelaere, R.H., Wasp, E.J., 1984. Fluid flow, slurry systems and pipe lines. In: Kirk-Othmer, Encyclopedia of Chemical Technology, third ed. Wiley Interscience.

Ergun, S., 1952. Fluid flow through packed columns. Chem. Eng. Prog. 48, 89–94.

Foscolo, P.V., Gibilaro, L.G., 1987. Fluid dynamic stability of fluidized suspensions, The particle bed model. Chem. Eng. Sci. 39, 1489–1500.

Ishida, M., Shirai, T., 1979. Velocity distributions in the flow of solid particles in an inclined open channel. J. Chem. Eng. Jpn. 12, 46–50.

Joseph, D.D., Singh, P., Fortes, A., 1991. Nonlinear and finite size effects in fluidized suspensions. UMSI report 91/232, August 1991, University of Minnesota.

Kim, I., Elgohbashi, S., Sirignano, W.A., 1993. Three-dimensional flow over two spheres in parallel side-by-side motion. J. Fluid Mech. 246, 465–488.

Nasr-El-Din, H., Shook, C.A., Colwell, J., 1987. A conductivity probe for measuring local concentrations in slurry systems. Int. J. Multiphase Flow 13, 365–378.

Richardson, J.F., Zaki, W.N., 1954. Sedimentation and fluidization: Part I. Trans. Inst. Chem. Eng. 32, 35–52.

Savage, S.B., 1979. Gravity flow of cohesionless granular materials in chutes and channels. J. Fluid Mech. 92, 53–96.

Schlichting, H., 1979. Boundary Layer Theory, seventh Ed. McGraw Hill, New York. 812pp, p. 238.

Shillen, D.J., Corrsin, S., 1975. Dispersion measurements in a turbulent boundary layer. Int. J. Heat. Mass Trans. 19, 285–295.

Shook, C.A., Roco, M.C., 1991. Slurry Flow: Principles and Practice. Butterworth-Heinemann, Boston. 324pp.

Taylor, G.I., 1953. Dispersion of soluble matter in solvent flowing slowly through a tube. Proc. Roy. Soc. A 219, 186–203.

Taylor, G.I., 1954a. The dispersion of solid matter in turbulent flow through a pipe. Proc. Roy. Soc. A 223, 446–468.

Taylor, G.I., 1954b. Conditions under which dispersion of a solute in a stream of solvent can be used to measure molecular diffusion. Proc. Roy. Soc. A, 473–477.